Coordination Chemistry Reviews, 104 (1990) 113–141
Elsevier Science Publishers B.V., Amsterdam

SPECTRAL, PHOTOPHYSICAL AND PHOTOCHEMICAL PROPERTIES OF $Ru(bpy)_3^{2+}$ ON POROUS VYCOR GLASS

HARRY D. GAFNEY

Department of Chemistry, City University of New York, Queens College, Flushing, NY 11367 (U.S.A.)

(Received 18 August 1989)

CONTENTS

A. INTRODUCTION

With the exception of crude oil, $Ru(bpy)_3^{2+}$ is one of the few reagents to benefit from the energy crisis. The need to develop alternative energy sources fueled an intense interest in its newly discovered excited state redox chemistry [1–3]. A number of systems were examined, but it was quickly apparent that two interrelated problems had to be resolved. Firstly the rapid exergonic back reactions accompanying photoinduced electron transfer must be curtailed, and secondly the one-photon–one-electron events must be converted into more useful multielectron events. Sacrificial reagents were found to prevent the back reaction and allow subsequent multielectron transfer events [2]. However, the system is not catalytic, but stoichiometric in the scavenger. Regeneration of the photoactive reagent is essential to catalytic activity. Consequently, research during the past decade has focused

0010-8545/90/$10.15

on imposing some constraint that allows charge separation to be competitive with an exergonic back reaction.

One approach is the use of heterogeneous media. As pointed out by Somorjai, the approach follows nature where many biological reactions, including photosynthesis, occur in, and to a significant extent are a consequence of the heterogeneity of the system [3]. Data gathered during the past decade show that a variety of heterogeneous media not only improve charge separation relative to homogeneous fluid media, but in some cases also allow an accumulation of electron density sufficient to drive subsequent multielectron transfer reactions [4–16]. Semiconductive metal oxides, for example, improve charge separation by electron injection into a bulk conduction band. Band bending is thought to curtail charge recombination, while the conduction band allows electron accumulation at removed reaction sites [10–14]. Inorganic oxide supports that are not considered charge conductors also promote charge separation [7,9,15,16]. In these systems, where population of a bulk conduction band is energetically unlikely, the increase in the lifetime of the charge-separated state appears to be the result of the order imposed by the rigid medium [15,16].

In the absence of an accessible conduction band, rigidity and topology are the advantages, and to a significant extent the fascination, of solid supports. Utilizing these characteristics to promote a specific behavior, however, requires an understanding of the nuances of microstructure and microenvironment. Surface characteristics, such as the nature and density of the surface functionalities and surface charge, determine the mechanism of adsorption, and in turn, the spectral and photophysical properties of the adsorbate. In cases where adsorbate mobility is curtailed, which is the case when $Ru(bpy)_3^{2+}$ is adsorbed onto hydroxylated silicas, clay and cellophane [7], the adsorbent defines an adsorbate array, and adsorbent topology and porosity determine access to the photoexcited adsorbate. Regardless of the specific nature of the support, or whether it is present as a bulk material, as in our case, or as a colloidal dispersion, the active region is the surface and the adjacent interface with the surrounding medium [7]. Consequently, the study of a photoexcited adsorbate is as much a study of the adsorbent surface as it is a study of the photophysics and photochemistry of the adsorbate [7].

Certainly in our case, the underlying strategy is to take advantage of the properties of a solid support to impose some control, principally kinetic, on an $Ru(bpy)_3^{2+}$-based reaction system. Yet the properties that differentiate a solid support from fluid solution, i.e. those properties that one is attempting to exploit, arise from the same properties that create the experimental difficulties. With many solids, the number of atoms, typically 10^{23} cm^{-3}, their close spacing, and the resulting band structure, limit optical transparency [17]. Support opacity is an experimental handicap since much of our

understanding of the excited states of ruthenium(II) diimmines, particularly their photoredox properties, arises from their spectroscopic visibility [1,2].

A number of years ago we began to explore the use of Corning's code 7930 porous Vycor glass (PVG) as a reaction medium. Our interest in PVG stems from its unique combination of rigidity, transparency and porosity. Transparency (50%T at 295 nm vs. air) offers spectroscopic access, and in turn, an amenability to optical spectroscopy and fast reaction techniques. Porosity offers chemical access; access not only in the sense of intercepting an excited state, but also in the chemical sense of utilizing the rigidity and topology of the glass surface to assemble a photochemical reaction site. This review describes the properties of this unusual reaction medium, and summarizes the photophysical and photochemical properties of $Ru(bpy)_3^{2+}$ adsorbed onto the medium.

B. POROUS VYCOR GLASS

Porous Vycor glass (PVG) is a 96% SiO_2, 3% B_2O_3 and 1% Al_2O_3 and Na_2O glass [18]. When the borosilicate melt is cooled below its phase transition point, the boron oxide–alkali oxide phase separates from the silica phase. The borate phase is acid leached, leaving a random three-dimensional array of interconnected pores. Small-angle X-ray scattering (SAXS) indicates a spinodal structure with a correlation length of 232 Å [19].

Pore size is defined by the extent of acid leaching and cavity sizes ranging from 20 to 2500 Å in diameter are available [18–32]. With cavity sizes greater than 100 Å, however, the glass appears opalescent and there is a concomitant reduction in transparency. The experiments described here are limited to a transparent (50%T at 295 nm vs. air) form of the glass containing 70 ± 21 Å diameter cavities. In these samples, the surface area is about 130 $m^2\ g^{-1}$, and the void volume, i.e. the volume of the cavities relative to the total sample volume, is about 30%.

Diffuse reflectance FTIR (DRIFT) spectra of the calcined (550°C) glasses reveal a surface composed of free, 3744 cm^{-1}, and associated, 3655 cm^{-1}, silanol groups [29,31,34]. In many of the calcined samples, however, a weak broad absorption due to chemisorbed water, 3500 cm^{-1}, is present, although its relative intensity is always 10% or less that of the silanol band [34]. The ζ potential of PVG in water, -26 mV, indicates an anionic surface relative to the bulk solvent [35], and the adsorption of acid–base indicators reveals a surface pH of 4–5 [36]. In both surface functionality and potential, PVG resembles silica gel [21,30,31], but one difference should be noted. Because of its method of preparation, PVG, unlike silica gel, possesses surface B_2O_3 Lewis acid sites [31]. The number of these sites

depends on the extent of acid leaching, but some estimates suggest that as much as one-third of the surface could be B_2O_3 [31].

Initial experiments were carried out with unpolished samples whereas later experiments were carried out with polished samples. The unpolished samples, or raw glass, have a wavy surface. The waves, which are referred to as chill marks, arise from the more rapid cooling of the external surfaces relative to the bulk. It is not possible to simply polish porous glass, since polishing fills the pore openings with debris. Rather, the glass is first polished and then acid leached. As a result, the surface of the polished samples is representative of the bulk, but different from the surface of the unpolished samples. The surfaces of both samples are anionic, and both possess free and associated silanol groups. However, the silanol number, i.e. the number of silanol groups per unit area, is not necessarily the same. Previous studies of a variety of hydroxylated silicas yield an average of 4–7 silanol groups per 100 $Å^2$, but also suggest that the silanol number is largest within the pores [29]. Consequently, the silanol number in the polished samples, where the surface is representative of the bulk, may be larger than that in the unpolished samples.

Another parameter, certainly of equal importance to the silanol number, is the surface topology. Beyond the obvious differences in macroscopic flatness of the polished and unpolished samples, scanning electron microscopy (Fig.1) reveals differences in the more relevant microscopic topology. The surface of the unpolished samples (Fig.1a) is composed of larger, interconnected glass nodules with crevices between the nodules. The crevices are of the order of 100 nm in width and contain the openings into the interior pores. The surface of the polished samples, however, is composed of smaller nodules (Fig.1b). The crevices between the nodules are approximately the same width as those in the unpolished samples, but owing to the smaller nodule size, the number per unit area is larger. Again, the openings into the interior pores lie within these crevices, but in many places, the openings appear as large indentations, which can be as wide as 1000 nm, in the glass surface. Some adsorption occurs onto the outermost surfaces of the glass nodules, but in both the polished and unpolished samples, the vast majority, of the order of 80–90%, of $Ru(bpy)_3^{2+}$(ads) (ads designates an adsorbed reagent) binds within the crevices or pore openings [37]. Consequently, the accessibility of the adsorbed complex to a quencher reflects, to a large extent, the topology of the glass surface.

(i) Impregnation

Like other hydroxylated silicas, PVG acts as a cation exchanger. Cationic complexes, such as $Ru(bpy)_3^{2+}$, displace the slightly acidic ($pK_a \approx 9$) silanol

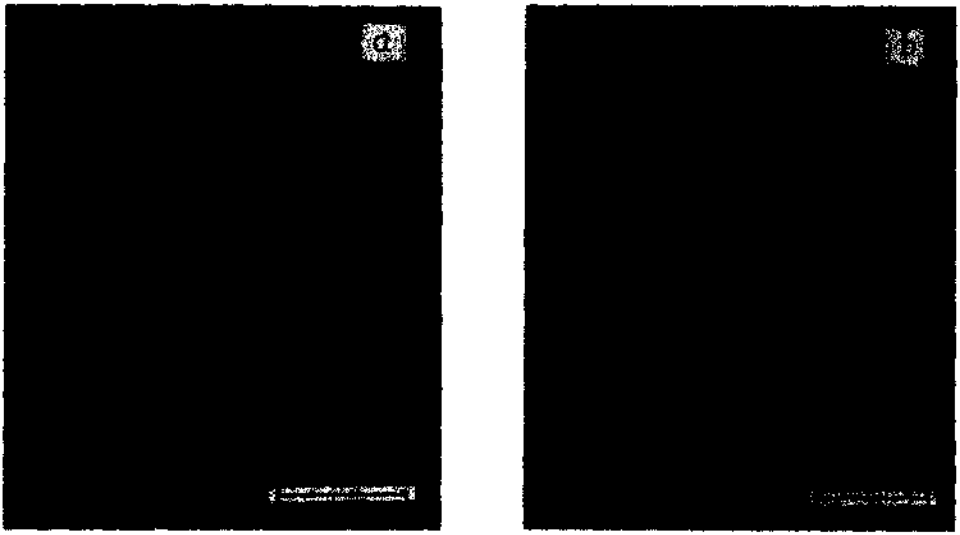

Fig. 1. Scanning electron micrographs of (a) unpolished and (b) polished porous Vycor glass. In each sample, the length scale (lower right) corresponds to 1.00 μm.

protons [21], and are adsorbed onto the glass without coadsorption of the counter-anions. Neutral complexes physisorb onto the glass [33,34,38], but anionic complexes are electrostatically repelled from the surface [39]. If the surface charge is reduced by first adsorbing alkali or alkaline earth cations, anionic complexes can be adsorbed. However, a large excess of the cation has to be adsorbed in order to obtain some adsorption of the anion [39]. As a result, it is not clear how this new surface is related to the original glass surface.

PVG offers two surfaces for adsorption; the outermost surfaces of the glass and the surfaces of the interconnected 70 ± 21 Å diameter cavities. Despite the availability of silanol groups throughout the glass [29,31], conventional solution impregnation techniques do not yield a uniform distribution of $Ru(bpy)_3^{2+}$ amongst these surfaces [37]. After removal of the water incorporated during impregnation, $Ru(bpy)_3^{2+}$(ads) is uniformly distributed amongst the outer surfaces, but not throughout the interior of the glass [37].

Adsorbate distribution reflects a number of factors, but with larger substitution-inert complexes such as $Ru(bpy)_3^{2+}$, size appears to be the principal factor [37]. Despite the relatively large pore diameter of 70 ± 21 Å, the rates of adsorption suggest that the narrower tortuous passes connecting the pores prevent diffusion into the interior regions of the glass. The initial penetration depth is achieved during the movement of the solvent front, and regardless of the moles adsorbed, $Ru(bpy)_3^{2+}$(ads) uniformly impregnates the volumes of glass defined by the area of a particular side and the penetration depth. In unpolished samples that are 5 mm thick, the

penetration depth is 0.45 ± 0.05 mm [37], but it is considerably shorter in the polished samples. Equivalent cross-sectional distributions occur with other large complexes that differ from $Ru(bpy)_3^{2+}$ in both size and mechanism of adsorption [33,34,40]. Thus larger complexes appear to clog these narrower constrictions and severely curtail transport into the bulk of the glass. $Ru(bpy)_3^{2+}$ will eventually impregnate the entire volume of PVG if the PVG is left in the impregnating solution over a period of months. For all practical purposes, however, the increase in penetration depth after 48 h is negligible [37]. As a result, the samples examined in our experiments are surface impregnated. The interior of the glass, about 90% of the total volume, remains vacant.

Particularly in a porous support, a non-uniform cross-sectional distribution of the adsorbate precludes an accurate calculation of surface coverage. Nevertheless, the parameter is valuable, since it can be used in a relative sense, and its estimation deserves some comment. Optical density measurements establish a uniform distribution of the complex in the impregnated volumes [37]. Taking 7.4 Å as the radius of $Ru(bpy)_3^{2+}$, and 130 $m^2\ g^{-1}$ and 1.38 g mL^{-1} as the surface area and density respectively, monolayer coverage in the impregnated volumes requires a loading equal to or greater than 10^{-4} mol g^{-1}. It is important to realize, however, that the surface coverages quoted below refer to that within the impregnated volumes of glass.

Unless otherwise specified, the experiments described below refer to "dry" samples in which 99.97% or more (by weight) of the water incorporated during impregnation has been removed under vacuum. $Ru(bpy)_3^{2+}$(ads) cation exchanges onto the glass and exists as an individual ion on a hydroxylated surface. In this sense, the molecular environment, although more rigid, is similar to that of the complex dissolved in aqueous solution. Impregnation is limited to the outermost volumes of glass, but within these volumes the majority of the complex, 90% or more, adsorbs into the crevices shown in Fig. 1. In spite of the relatively small portion of the glass impregnated, the problem is not increasing the amount adsorbed, but controlling the amount adsorbed so that the impregnated sample retains sufficient transparency for spectral examination.

C. SPECTROSCOPIC PROPERTIES

Whether adsorbed into interior cavities or, as is the more common situation, adsorbed into the crevices in the outermost volumes of glass, the spectroscopic properties of the molecule are equivalent. In the 300–500 nm region, the UV–visible spectrum of $Ru(bpy)_3^{2+}$(ads) is within experimental error in band maxima, relative extinction coefficient, and band half-width of

the spectrum of the complex in aqueous solution [41]. Absolute extinction coefficients, calculated assuming an optical path length equivalent to the penetration depth, are 10–15% larger than those in aqueous solution. The actual difference is most likely smaller, however, since differences in light scattering, due to the random array of pores in the glass, introduce an inherent spectroscopic uncertainty of 8% from sample to sample, and there is an uncertainty of about 20% in the penetration depth [41]. The latter describes the cross-sectional distribution in the general sense, but is not an accurate measure of optical path length.

Resonance Raman spectra of $Ru(bpy)_3^{2+}$(ads) show that the seven bipyridine vibrations resonant with the 452 nm metal-to-ligand charge transfer (MLCT) transition differ by 1 cm^{-1} or less from those in the aqueous solution spectrum. However, the intensity of the prominent 1492 cm^{-1} vibration is reduced by 44% relative to that in the aqueous solution spectrum [41]. Frequency is a ground state property, whereas intensity is related to the origin shift, i.e. the shift in the equilibrium position of a particular normal mode on excitation from ground to excited state [42]. Being the most intense band in both spectra, the 1492 cm^{-1} vibration plays a major role in converting the ground state structure to that of the excited state. The implication, of course, is that the ground state structure of $Ru(bpy)_3^{2+}$(ads) is equivalent to that in aqueous solution, whereas the excited state structure differs from that in water. It should be emphasized that these spectra probe the structural changes that accompany the allowed 452 nm transition that populates the MLCT state prior to intersystem crossing to the emissive state. Nevertheless, the rigidity of PVG, as opposed to the fluidity of water, appears to curtail the molecular distortions that accompany electronic excitation to the spin-allowed MLCT state [41].

Although the amplitude of the 1492 cm^{-1} vibration changes, there is little effect on the emission energy. The emission maximum of $Ru(bpy)_3^{2+}$(ads) occurs at 610 nm, as compared with 600 nm in water [41]. The emission band shapes are equivalent in both media and the shift is similar to that on changing from one solvent to another. The excited state redox potentials are taken as the difference between the emission energy, which is essentially unaffected by adsorption, and the ground state redox potentials. Absorption and resonance Raman spectra establish that the ground state of $Ru(bpy)_3^{2+}$(ads) is equivalent to that in aqueous solution. Assuming the ground state redox potentials are unchanged by adsorption, since these are essentially independent of solvent, the excited state redox potentials for the adsorbed complex are taken to be equivalent to those in aqueous solution [2]:

$$*Ru(bpy)_3^{2+}(ads) \rightarrow Ru(bpy)_3^{3+}(ads) + e^- \qquad E=0.88\ V \qquad (1)$$

$$e^- + *Ru(bpy)_3^{2+}(ads) \rightarrow Ru(bpy)_3^{+}(ads) \qquad E=0.77\ V \qquad (2)$$

Energetically, the excited state redox chemistry accessible on the glass is equivalent to that accessible in aqueous solution.

D. EXCITED STATE DYNAMICS

The quantum yield of $Ru(bpy)_3^{2+}$(ads) emission, Φ_{em}, depends on whether the glass surface is polished or unpolished. With unpolished samples, the emission quantum yield in vacuo ($p \leqslant 10^{-4}$ Torr) at room temperature ($22 \pm 1°C$) is 0.12 ± 0.02 [41], whereas that on a polished sample is 0.078 ± 0.004 [43]. The emission lifetime of $Ru(bpy)_3^{2+}$(ads), however, is independent of whether the surface is polished or unpolished. The difference in Φ_{em} is not a consequence of a molecular change. The complex cation exchanges onto the outermost surfaces of both samples, and the absorption, emission and resonance Raman spectra of the complex on both surfaces are equivalent. The data described below have, for the most part, been obtained with the complex adsorbed onto polished samples. While the absolute value of Φ_{em} differs, the relative changes are within experimental error for both the polished and unpolished samples.

With 10^{-4} mol or more $Ru(bpy)_3^{2+}$(ads) per gram, Φ_{em} declines with increasing loading [41]. The decline is attributed to self-quenching since it occurs under low excitation intensities and at essentially monolayer coverage in the impregnated regions. With samples containing less than monolayer coverage, equal to or less than 10^{-4} mol g^{-1}, Φ_{em} is independent of loading [41]. The emission lifetime τ is also independent of loading [41], but at all loadings of 10^{-4} mol g^{-1} or less, τ exhibits a pronounced dependence on excitation intensity [43,44]. With low intensity excitation, principally 337 and 358 nm pulses (2–5 ns, FWHM) from an Ortec nanosecond pulser, the emission decay of $*Ru(bpy)_3^{2+}$(ads) in vacuo at room temperature is exponential and yields an emission lifetime of 740 ± 20 ns [41]. As the excitation intensity increases, a rapid ($t \leqslant 50$ ns) non-exponential component precedes the slower exponential decay [44]. With 355 nm laser excitation, the ratio of the intensity of the rapid component relative to that of the slower exponential decay, I_f/I_s at $t=0$, is proportional to the square of the excitation power, but declines with increasing loading [44]. The decline in the intensity ratio precludes triplet–triplet annihilation since the latter would be expected to increase with increasing loading. Furthermore, triplet–triplet annihilation is inconsistent with a pronounced blue shift in the emission spectrum. With high intensity 355 nm excitation (14 mJ $pulse^{-1}$), the emission spectrum constructed from the decay data exhibits a maximum at 510 nm with a distinct shoulder at 610 nm [44]. The measured lifetime of the 610 nm component reflects the preceding non-exponential component, but in all

experiments the decay is exponential and occurs with a lifetime ranging from 700 to 750 ns. Since the emission maximum agrees with the solution emission maximum and its decay is exponential, the 610 nm component is assigned to the well established radiative decay of the triplet MLCT state [44]. The emission lifetime is taken to be that measured under low intensity excitation, 740 ± 20 ns [41].

The cause of the 510 nm emission is not clear. Blue shifts have been reported when the complex is adsorbed onto silica gel, but the magnitude of the shift, about 1100 cm^{-1} [45], is considerably smaller than the shift of about 3200 cm^{-1} found here [44]. The 510 nm emission is proportional to the square of the excitation intensity, and other experiments (see below) show that biphotonic excitation of $Ru(bpy)_3^{2+}$(ads) leads to photoionization [46]. We suspect that the 510 nm emission arises from a chemiluminescent reaction of the photodetached electron on the glass surface [46]. It is not simply charge recombination, however, since the reduction of $Ru(bpy)_3^{3+}$ in aqueous solution by the hydrated electron leads to the conventional 600 nm emission, which decays exponentially [47]. More likely, it arises from a reaction of the photodetached electron with some at present unknown site on the glass surface.

The emission quantum yield and lifetime of $Ru(bpy)_3^{2+}$(ads) in vacuo ($p \leqslant 10^{-4}$ Torr) at room temperature (22 ± 1°C), and the radiative and non-radiative rate constants derived from these parameters are summarized in Table 1. A comparison of the values obtained for the adsorbed complex with those measured in aqueous solution (Table 1) shows that the increase in Φ_{em} is not accompanied by an equivalent increase in τ. The room temperature value Φ_{em} is 1.7 times larger than that in degassed water, whereas the emission lifetime τ is only 1.2 times larger. Consequently, adsorption onto the glass does not increase Φ_{em} simply by reducing the non-radiative rate of relaxation. The non-radiative rate constants in the two media are similar, perhaps reflecting the fact that non-radiative decay in both media involves a vibronic coupling through similar O–H vibrations. Rather, adsorption onto

TABLE 1

Photophysical parameters of $Ru(bpy)_3^{2+}$ on porous Vycor glass and in aqueous solution[a]

Medium	Φ_{em}	t (ns)	k_r[b] (10^4 s^{-1})	k_{nr}[b] (10^6 s^{-1})
PVG[c]	0.078 ± 0.004	740 ± 20	18.0 ± 1.0	1.2 ± 0.1
H_2O	0.042 ± 0.002	580 ± 19	7.2 ± 0.3	1.6 ± 0.1

[a]Measured at room temperature 22 ± 1°C either under vacuo ($p \leqslant 10^{-4}$ Torr) or in degassed aqueous solution. [b]Calculated assuming that η_{isc} is unity (see text). [c]Polished samples.

this glass leads to increases in the radiative rate constant, and causes fundamental changes in the relaxation processes.

Much of our understanding of the excited state processes in $Ru(bpy)_3^{2+}$ arises from the temperature dependence of Φ_{em} and τ. In H_2O and D_2O, intersystem crossing from the states populated on absorption to the emissive MLCT state, η_{isc}, is unity and independent of temperature [48]. Relaxation of the emissive MLCT state involves temperature independent radiative and non-radiative decay that directly couple the emissive MLCT state with the ground state, and a temperature dependent non-radiative pathway [48]. The temperature dependence arises from the population of ligand field (LF) manifold that lies about 3600 cm^{-1} above the MLCT state. Similar models, but with an additional Arrhenius term and slight changes in the MLCT–LF energy gap, account for the temperature dependence of emission lifetime in other solvents [49], and for the decay of mixed-ligand complexes [50].

In the 278–363 K range, absorption and emission spectra of $Ru(bpy)_3^{2+}$(ads) are in excellent agreement with aqueous solution spectra [43]. However, the temperature dependence of Φ_{em} and τ differs from that in aqueous solution (Fig. 2). Unlike in aqueous solution, where intersystem crossing and the radiative constant are independent of temperature, one or both of the parameters are temperature dependent when the complex is adsorbed onto PVG. The decline in η_{isc} and/or k_r with increasing temperature is not an experimental artifact. The refractive index of PVG is independent of temperature in the 0–100°C range. Self-quenching requires essentially monolayer coverage, equal to or greater than 10^{-4} mol g^{-1} [41], whereas the samples used to determine the temperature dependence of Φ_{em} and τ contain from 5×10^{-7} to 5×10^{-6} mol g^{-1} which correspond to surface coverages of 0.5–5% in the impregnated volumes of glass. Increasing the temperature could increase adsorbate mobility, and promote self-quenching at less than monolayer coverage. However, the polarization ratios for $Ru(bpy)_3^{2+}$(ads) measured at room temperature (Table 2) are within experimental error of those measured in 77 K ethanol glasses [41], and independent of temperature over the 5–90°C range (Fig. 3) [52]. Furthermore, since the results are reproducible from sample to sample, and independent of whether the sample is calcined in air or under H_2 [43], a subtle form of temperature-dependent impurity quenching is unlikely.

It is not surprising, in view of this fundamental change, that the current solution phase models do not account for the temperature dependence shown in Fig. 2. In fact, attempts to fit the Van Houten–Watts model [48] to the data by varying the MLCT-LF energy gap from 1000 to 8000 cm^{-1} fail to reproduce the observed temperature dependence on the glass. The MLCT-LF energy gap cannot be measured directly, but larger variations in the energy gap seem rather arbitrary, in our opinion, without a concurrent

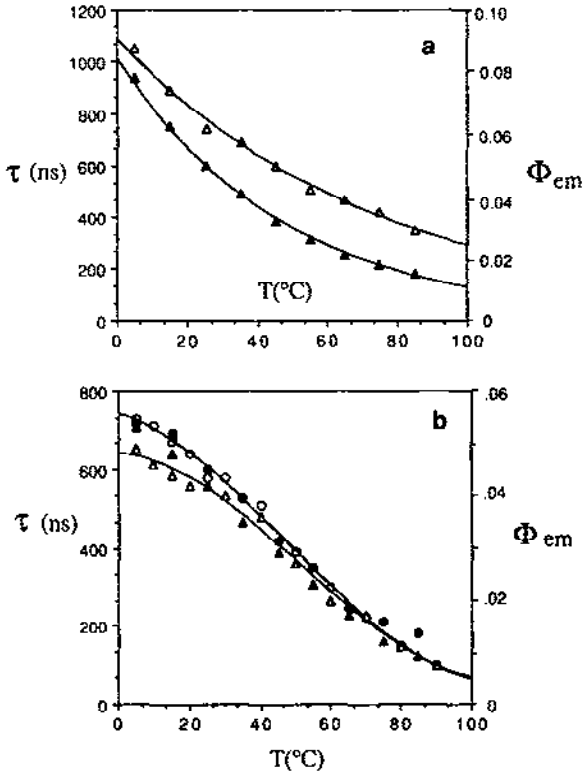

Fig. 2. (a) Temperature dependence of emission quantum yield, Φ_{em} (△) and lifetime (▲) for the adsorbed complex. (b) Temperature dependence of emission quantum yields (▲) and lifetimes (●) in degassed aqueous solution. Emission quantum yields (△) and lifetimes (○) reported by Van Houten and Watts [48] are also included.

TABLE 2

Emission polarization ratios

Medium	Excitation wavelength (nm)		
	400	465	510
PVG[a]	0.10±0.01	0.16±0.02	0.10±0.01
77 K ethanol[b]	0.08	0.20	0.10

[a]Measured at room temperature, 22±1°C, in vacuo. [b]Reported error, 10% [79].

change in the complex's absorption spectrum. Over the entire temperature range examined, however, the absorption spectrum of $Ru(bpy)_3^{2+}$(ads) closely parallels that of the complex in aqueous solution [43].

Experiments are being performed to determine whether k_r or η_{isc} or both

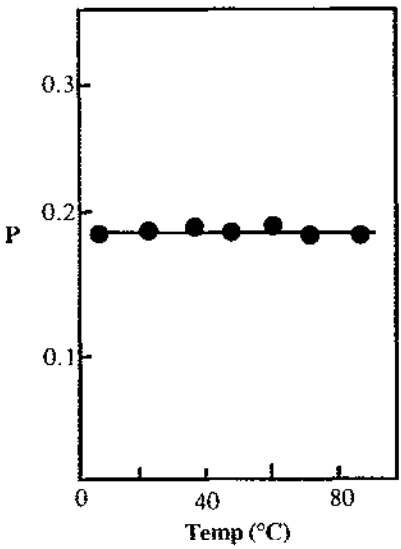

Fig. 3. Emission polarization ratios, P, for $Ru(bpy)_3^{2+}$(ads) as a function of temperature. Samples contain $(2.0 \pm 0.1) \times 10^{-6}$ mol g^{-1}; excited with 465 nm light and emission monitored at 600 nm.

are temperature dependent. Nevertheless, a number of points can be made at this juncture. Since the product declines with increasing temperature, the proposal of an intervening activation step, particularly with energy-rich, excited states, appears to us to be more of a computational convenience rather than an indication of what is actually happening. At present, it seems more likely that the decline reflects a change in the vibrational overlap which couples one state to another, and may be related to structural differences indicated by the resonance Raman spectra [41]. If η_{isc} declines with temperature, then the measured emission quantum yields and the corresponding radiative rate constants are lower limits of the true values, particularly at higher temperatures. Considering the ever-widening use of the complex as a luminescent probe of relatively rigid solid supports and less rigid chemical and biochemical polymers, detailing the effect of the medium on the excited state dynamics seems essential.

E. QUENCHING

Energetically, the excited state chemistry accessible on the glass is equivalent to that in fluid solution. However, emission polarization and macroscopic distribution measurements establish that $Ru(bpy)_3^{2+}$(ads) is immobilized on the glass surface [37,41]. The absence of adsorbate mobility distin-

guishes this and other supports [53,54] from homogeneous fluid solution. If the reagents are immobilized or their mobility is negligible during the $^*Ru(bpy)_3^{2+}$(ads) lifetime, which is 740 ± 20 ns on this glass, quenching becomes a function of adsorbate array. In this sense, a porous support is analogous to a chromatography column, where quenching reflects the factors that control the partitioning of the reagents either within the support or amongst different phases. Quenching of $Ru(bpy)_3^{2+}$(ads) by gases, or across an aqueous–non-aqueous interface at the glass surface, for example, are functions of the partitioning of reagents amongst different phases, whereas quenching by coadsorbed metal ions examines partitioning within the support.

(i) Quenching by gases

O_2, N_2O and SO_2 quench $^*Ru(bpy)_3^{2+}$(ads) [55]. While the low energy of singlet O_2 precludes an energetic distinction as to mechanism [56,57], the relatively high excited state energies of N_2O [58] and SO_2 [59], equal to or greater than 3.2 eV, indicate an electron transfer process. The mild oxidizing properties of N_2O towards low oxidation state transition metals suggest an oxidative process

$$^*Ru(bpy)_3^{2+}(ads) + N_2O \rightarrow Ru(bpy)_3^{3+}(ads) + N_2O^- \quad (3)$$

whereas the reducing properties of SO_2 suggest a reductive mechanism

$$^*Ru(bpy)_3^{2+}(ads) + SO_2 \rightarrow Ru(bpy)_3^{+}(ads) + SO_2^+ \quad (4)$$

Neither reaction leads to a net chemical change, indicating that both are followed by rapid exergonic back reactions [55].

In the quenching of an adsorbed molecule by a gaseous reagent, two limiting conditions exist. Firstly, quenching is due to the gaseous molecules impinging onto the surface. Secondly, the gas molecules adsorb and quenching occurs between coadsorbed molecules. In the first case, quenching is proportional to the rate at which the gas molecules collide with the surface. The flux of molecules impinging onto the surface per second per square centimeter is $P/(2\pi mkT)^{1/2}$, where P, m, k and T are the pressure of the gas, its molecular mass, the Boltzmann constant, and the temperature respectively [60]. In these experiments where the $Ru(bpy)_3^{2+}$(ads) loading of $(1.0 \pm 0.2) \times 10^{-6}$ mol g^{-1} corresponds to a surface coverage of 2% or less, only that fraction of the gaseous molecules that either collides with the adsorbed complex or collides within a quenching radius is actually effective. Nevertheless, quenching due solely to the flux of gaseous molecules onto the surface exhibits a linear dependence on gas pressure. With each gas, quenching is initially proportional to the pressure, but all exhibit regions

where it becomes independent of gas pressure [55]. Moreover, the quenching of different samples of $Ru(bpy)_3^{2+}$(ads) is not a reproducible function of the gas pressure, but is a reproducible function of the moles of each gas adsorbed. Consequently, adsorption precedes quenching, and quenching occurs principally between coadsorbed reagents [55].

With N_2O, the equivalence of the intensity and lifetime quenching data establishes a dynamic process [55]. Dynamic quenching implies either a long-range interaction or, since $*Ru(bpy)_3^{2+}$(ads) is immobilized, N_2O(ads) is mobile on the glass. Being weakly adsorbed and a mild oxidant with little driving force for a long-range interaction, dynamic quenching by N_2O(ads) is attributed to the mobility of N_2O(ads) on the glass surface. Although not directly comparable to fluid solution, the magnitude of the quenching rate constant, 5.3×10^9 mol^{-1} s^{-1}, suggests that N_2O(ads) is relatively mobile. The majority of $Ru(bpy)_3^{2+}$(ads), of the order of 80–90%, adsorbs into the crevices on the glass surface (Fig. 1), and excitation produces a gradient of excited states into the glass matrix. The small fraction quenched, 28% or less suggests that N_2O(ads) mobility is not throughout the entire glass matrix, but is limited to the outermost surfaces of the glass where it has access to a relatively small fraction of $*Ru(bpy)_3^{2+}$(ads) [55].

With O_2(ads) and SO_2(ads), 70% or more of the quenching occurs by a static process [55]. Since the absorption spectrum of $Ru(bpy)_3^{2+}$(ads) is unaffected by the gases, and the adsorption isotherms of these gases are independent of the presence of $Ru(bpy)_3^{2+}$(ads), static quenching does not involve the formation of a precursor complex. Adsorption of SO_2 and of O_2 are random processes, and quenching of the adsorbed complex is analogous to static quenching in frozen homogeneous solution [61] where

$$I_0/I=(1+K_{SV}[Q])\exp(k'[Q]) \tag{5}$$

I and I_0 are the steady state emission intensities in the presence and absence of the gas, K_{SV} is the Stern–Volmer constant, and k' is the constant for static quenching. Since quenching is limited to coadsorbed molecules, $[Q]$ represents the moles of gas adsorbed per gram of PVG. Substitution of t_0/t for the dynamic component yields

$$\ln(I_0/I)(t/t_0)=k'[Q] \tag{6}$$

Taking k' to be AN where A is the surface area of the glass and N is the molecules of gas adsorbed per unit surface area, the donor–quencher interaction distance is related to k' in eqn. (6) by

$$r=(k'/f\pi N)^{1/2} \tag{7}$$

Since it is not known whether the gas diffuses throughout the entire pore volume, f cannot be determined with certainty. Limits of r can be calculated,

however, by assuming that the gas either distributes throughout the entire pore volume, $f=1$, or since both gases quench 70% or more of the $^*Ru(bpy)_3^{2+}$(ads), O_2 and SO_2 impregnate the same volumes of glass as $Ru(bpy)_3^{2+}$(ads). In this case, f is 0.28. Within these limits, eqn. (7) yields 11 ± 1 Å $\leqslant r \leqslant 17\pm2$ Å and 27 ± 2 Å $\leqslant r \leqslant 42\pm4$ Å for O_2 and SO_2 respectively. The values are surprisingly large, but not that different from previous determinations of energy transfer and electron transfer quenching radii in hydrocarbon glasses at 77 K [62–64].

(ii) Quenching across an aqueous–non-aqueous interface

In deaerated acetonitrile, 2-methyl-1,4-naphthoquinone (MNQ), 1,4-naphthoquinone (NQ) and *p*-benzoquinone (BQ) quench $^*Ru(bpy)_3^{2+}$(ads). The quenching rate constants parallel the standard reduction potentials of the quinones (Table 3), and quenching is attributed to an oxidative process

$$^*Ru(bpy)_3^{2+} + Q \rightarrow Ru(bpy)_3^{3+} + Q^- \quad (8)$$

where Q and Q^- represent the quinone and its reduced analogue. No net chemical change occurs due to rapid (rate constant $\geqslant 2\times10^9$ M^{-1} s^{-1}) thermal back reactions [35].

Saturating samples of PVG containing $(3.84\pm0.60)\times10^{-7}$ mol $Ru(bpy)_3^{2+}$(ads) per gram with distilled water and immersing the sample in benzene interposes an aqueous–non-aqueous interface at the glass surface [35]. BQ is slightly soluble in water and when added to the benzene phase,

TABLE 3

Quenching by the different quinones in acetonitrile and across an aqueous–non-aqueous interface

Quinone	E^{0a} (V)	$k_q{}^b$ (10^9 M^{-1} s^{-1})	Na^+ (ads)^c (10^4 mol)	K	f_q
MNQ	0.422	3.10 ± 0.19	0	$\leqslant 10$	$\leqslant 0.01$
			0.3 (0.06)	68 ± 11	0.184
			1.0 (0.21)	82 ± 12	0.344
			2.2 (0.45)	93 ± 10	0.448
			4.0 (0.83)	114 ± 12	0.612
NQ	0.485	6.46 ± 0.20	0	102 ± 11	0.452
			1.0 (0.22)	141 ± 15	0.445
BQ	0.699	10.4 ± 0.2	0	60 ± 10	0.579
			1.0 (0.25)	68 ± 11	0.579

[a]For $Q+2e^-+2H^+ \rightarrow QH_2$ [80]. [b]Bimolecular quenching rate constants in CH_3CN. [c]Moles of Na^+ adsorbed per sample; values in parentheses are moles per gram of PVG.

30% of the quenching of the adsorbed complex occurs by a dynamic process with a rate constant of $(7.76 \pm 0.96) \times 10^8$ M^{-1} cm^{-1}. Since $Ru(bpy)_3^{2+}$(ads) remains bound to the glass surface, the rate constant reflects only the diffusion of BQ from the benzene phase into the aqueous phase. Relative to the rate constant in acetonitrile, it suggests that the interface retards diffusion.

The balance of the quenching by BQ and all the quenching by NQ occur by a static process. Consequently, these reagents partition amongst the phases and are within a quenching distance at the moment of excitation. Surprisingly, no quenching occurs when MNQ is added to the benzene phase even though the quenching reaction is exergonic by about 1.3 V, and in acetonitrile, MNQ quenches with a rate constant similar to that of NQ. Clearly, this is not an energetic distinction, but a distinction imposed by the interface, i.e. formation of the donor–quencher pair responds to the factors that control the partitioning of the quinone between the aqueous and benzene phases. Measurements of the ζ potential of the glass in water show that adsorption of an alkali metal ion reduces the thickness of the surface water layer [3]. Of these quinones, MNQ is the least soluble in water, and exhibits little tendency to penetrate the aqueous layer. Consequently, formation of the donor–quencher pair is prevented and quenching does not occur. In contrast, reducing the thickness of the aqueous layer would facilitate the formation of the donor–quencher pair. Indeed, coadsorption of Na^+ triggers quenching by MNQ, and the fraction quenched, f_q (Table 3), increases in proportion to the amount of Na^+ adsorbed onto the glass (Fig. 4). The effect is not specific to Na^+, and coadsorption of the ion does not affect the spectral properties of $Ru(bpy)_3^{2+}$(ads) or its emission lifetime [35]. Rather, its effect is to reduce the thickness of the surface aqueous layer, which allows MNQ to diffuse to within the necessary distance for adsorption and static quenching.

Static quenching implies that the quinones adsorb onto the support prior to excitation. However, this raises the question as to whether adsorption is random or biased by the presence of $Ru(bpy)_3^{2+}$(ads). Since there is little driving force for a long-range interaction, we assume that a contact interaction is necessary for quenching to occur. If adsorption is random, only that fraction within an effective quenching distance will be effective. Therefore the effective fraction is the ratio of the area defined by the molecular dimensions relative to the total surface area. The molecular dimensions define a circular area with a radius equal to the radius of $Ru(bpy)_3^{2+}$(ads), 7.4 Å, plus, assuming that it is free to rotate, twice the molecular length of the adsorbed quinone, 12.7 Å. Relative to the total surface area in the volumes of glass impregnated with the complex, the ratio indicates that about 13% of the randomly adsorbed quinone will be effective. For 50% quenching, random adsorption requires the adsorption of 2.5×10^{-5} mol quinone. The latter is

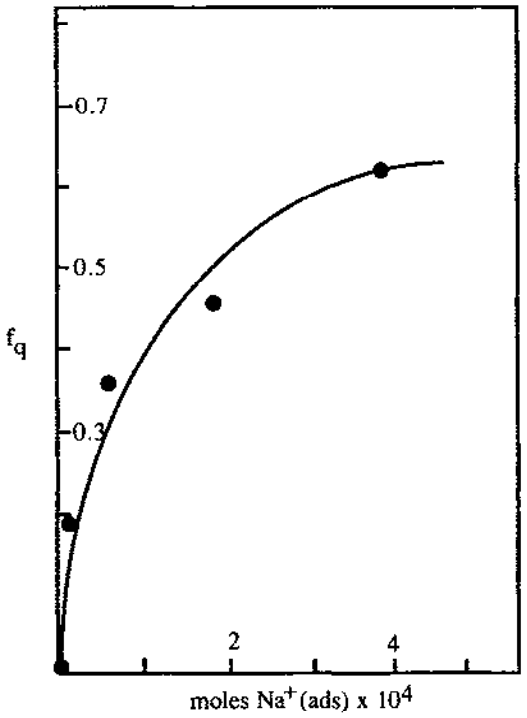

Fig. 4. Fraction of $*Ru(bpy)_3^{2+}$(ads) quenched (f_q) by MNQ as a function of Na^+(ads).

significantly larger than the 4.5×10^{-7} mol or less of quinone which spectral data indicate are adsorbed. Consequently, random adsorption is discounted. In fact, NQ and MNQ, which are insoluble in water, show little tendency to penetrate the aqueous layer and adsorb onto the polar hydrated surface of the glass. We have proposed that the quinones adsorb directly onto $Ru(bpy)_3^{2+}$(ads). The bipyridine ligands are hydrophobic and the adsorbed complex is either a hydrophobic nodule or creates hydrophobic regions in the surface crevices on an otherwise polar hydrated surface [35].

Direct adsorption is described by the equilibrium

$$Ru(bpy)_3^{2+}(ads) + Q \overset{K}{\rightleftharpoons} [Ru(bpy)_3^{2+},Q](ads) \tag{9}$$

Q represents the quinone in the benzene phase, and $[Ru(bpy)_3^{2+},Q](ads)$ represents the adsorbed donor–quencher pair. Excitation of the donor–quencher pair results in instantaneous quenching. Therefore the fraction of $*Ru(bpy)_3^{2+}$(ads) quenched is equivalent to the fraction of exciting light absorbed by $[Ru(bpy)_3^{2+},Q](ads)$:

$$(I_0 - I)/I_0 = 1 - \exp(-2.303\varepsilon' P) \tag{10}$$

I and I_0 are the emission intensities in the presence and absence of the quinone respectively. ε' is taken as the molar cross-sectional extinction coefficient of $Ru(bpy)_3^{2+}$(ads), 1.48×10^7 cm^2 mol^{-1}, since adsorption of the quinone does not affect its visible spectrum. Describing the moles of quinone adsorbed per square centimeter, P, by a Langmuir adsorption isotherm and substituting into eqn. (10) yields

$$(\ln(I_0/I))^{-1} = 1/k + 1/(kK[Q]) \tag{11}$$

K is the equilibrium constant for direct adsorption (eqn. (9)), and $k = 2.303\varepsilon' ab$, where a and b are proportionality constants (units, mol g^{-1} and g cm^{-2} respectively). Plots of $(\ln(I_0/I))^{-1}$ vs. $1/[Q]$ are linear and yield values of K (Table 3) which indicate that BQ and NQ have similar affinities for adsorption onto $Ru(bpy)_3^{2+}$(ads). The values of K for MNQ are proportional to the amount of Na^+(ads). While the effect of Na^+ appears in the equilibrium constant, it is important to realize that its effect is one of reducing the thickness of the surface aqueous layer and allowing MNQ to diffuse to within a distance for adsorption to occur [35].

Quenching across an aqueous–non-aqueous interface depends on the solubility of the quencher in the different phases. When the solubility difference is small, as with BQ, the quencher partitions between the phases and that fraction within the polar phase dynamically quenches the adsorbed complex. If the solubility difference is large, adsorption precedes quenching. Because of the polarity of the glass surface, adsorption appears to be specific to the hydrophobic regions created by the adsorbed complex. Whether random or specific, however, quenching becomes a function of the parameter(s) that control the partitioning of the quencher amongst the different phases.

(iii) Quenching by coadsorbed metal ions

In aqueous solution, Cr^{3+}, Fe^{3+} and Cu^{2+} quench $*Ru(bpy)_3^{2+}$ by dynamic essentially diffusion-controlled processes. When coadsorbed onto glasses containing $Ru(bpy)_3^{2+}$, however, quenching occurs by a static process [37]. Since $Ru(bpy)_3^{2+}$(ads) is immobilized on the glass [41], static quenching implies that the mobility of the coadsorbed ion is severely curtailed, at least during the $*Ru(bpy)_3^{2+}$(ads) lifetime of 740 ± 20 ns. The glass acts like a miniature chromatography column, and quenching reflects the distribution of the adsorbates within the glass.

Size appears to be the principal determinant of the distribution of larger substitution-inert complexes such as $Ru(bpy)_3^{2+}$. The narrow tortuous passes connecting the pores curtail diffusion into the interior pores, and under normal impregnation conditions, the complex uniformly impregnates

the outermost volumes of glass without penetrating more than a few tenths of a millimeter into the glass. The interior of the glass, generally about 90% of the total volume, remains vacant [37].

Size is not the determinant of the distribution of Cr^{3+}, Fe^{3+} and Cu^{2+}. The relative size of the fully hydrated ion increases in the order $Cu^{2+} < Cr^{3+} < Fe^{3+}$, while the depth of penetration into the glass increases in the order $Cr^{3+} < Fe^{3+} < Cu^{2+}$. Each metal ion cation exchanges onto the glass [46,65,66], but Cr^{3+} adsorbs onto the outermost surfaces of the glass, while Fe^{3+} impregnates essentially the same volumes of glass as $Ru(bpy)_3^{2+}$. In samples containing $Ru(bpy)_3^{2+}$(ads) at a concentration of $(5.0 \pm 0.2) \times 10^{-7}$ mol g^{-1}, which corresponds to a surface coverage of 2% or less in the impregnated volumes, the distributions of Cr^{3+}(ads) and Fe^{3+}(ads) are unaffected by the coadsorbed complex and are equivalent to that in the calcined glass [37].

Cu^{2+} distributes in a different manner and its distribution depends on the presence of $Ru(bpy)_3^{2+}$(ads). Regardless of the initial loading, which in these experiments ranged from 5×10^{-7} to 6×10^{-4} mol g^{-1}, Cu^{2+} uniformly distributes throughout the entire glass sample. In samples containing 5×10^{-7} mol $Ru(bpy)_3^{2+}$(ads) per gram and 5×10^{-5} mol or less Cu^{2+} per gram, however, Cu^{2+} partitions into the unoccupied volumes and uniformly impregnates the interior of the glass. Partitioning is not a result of saturating the outermost volumes of the glass with $Ru(bpy)_3^{2+}$(ads). Monolayer coverage within these volumes is readily achieved, and requires concentrations equal to or greater than 10^{-4} mol g^{-1}. The $Ru(bpy)_3^{2+}$(ads) loadings in these samples correspond to a surface coverage of 2% or less. Initially, Cu^{2+} impregnates the interior unoccupied volumes of glass. As the amount of Cu^{2+} adsorbed increases, however, the ion begins to impregnate the volumes of glass containing $Ru(bpy)_3^{2+}$(ads), and with concentrations equal to or greater than 2×10^{-4} mol g^{-1}, Cu^{2+} uniformly impregnates the entire glass sample [37].

The distributions of these ions parallel their kinetic labilities and the strength of the interaction with the glass surface [65–67]. Cu^{2+}, with an ionic potential of 2.00 is the least strongly bound, whereas Cr^{3+}, with an ionic potential of 4.69, is the most strongly bound. The value of 4.49 for Fe^{3+} suggests a somewhat weaker interaction than that of Cr^{3+}, but significantly stronger than that of Cu^{2+}. The rate constant for water exchange is 10^{-6} s^{-1} for Cr^{3+}, whereas those for Fe^{3+} and Cu^{2+} are 10^4 s^{-1} and 10^9 s^{-1} respectively. Apparently, Cu^{2+}, because of its weaker interaction with the glass surface and high lability, exchanges from site to site and rapidly diffuses into the interior of the glass, whereas Cr^{3+}, because of its stronger interaction with the surface and slow exchange rate, remains where first adsorbed, namely, at the external surfaces of the sample. Fe^{3+},

being somewhat intermediate, penetrates slightly and achieves a distribution similar to that of $Ru(bpy)_3^{2+}$(ads).

Static quenching by these coadsorbed ions reflects their distributions and how that distribution varies with the moles adsorbed. With Cr^{3+}, impregnation is limited to the outer surfaces, and quenching occurs only in those regions containing both reagents. Increasing the amount of Cr^{3+}(ads) does not increase the penetration depth. Consequently, the added ions do not have access to $*Ru(bpy)_3^{2+}$(ads), and quenching (Fig. 5a) becomes essentially independent of the moles adsorbed (equal to or greater than 3×10^{-6} mol g^{-1}). The distribution of Fe^{3+}(ads) is essentially equivalent to that of $Ru(bpy)_3^{2+}$(ads), and the relative emission intensity is a linear function of the moles adsorbed (Fig. 5b).

With 5×10^{-5} mol or less Cu^{2+}(ads) per gram, Cu^{2+} partitions into the interior of the glass where no $Ru(bpy)_3^{2+}$(ads) is present (see above). Partitioning prevents the formation of the donor–quencher pair, and quenching is initially independent (Fig. 5c) of the moles of Cu^{2+}(ads). As the moles of Cu^{2+}(ads) increase, however, the ion begins to impregnate the volumes of glass containing $Ru(bpy)_3^{2+}$(ads) and quenching (Fig. 5c) becomes proportional to the amount of Cu^{2+} adsorbed.

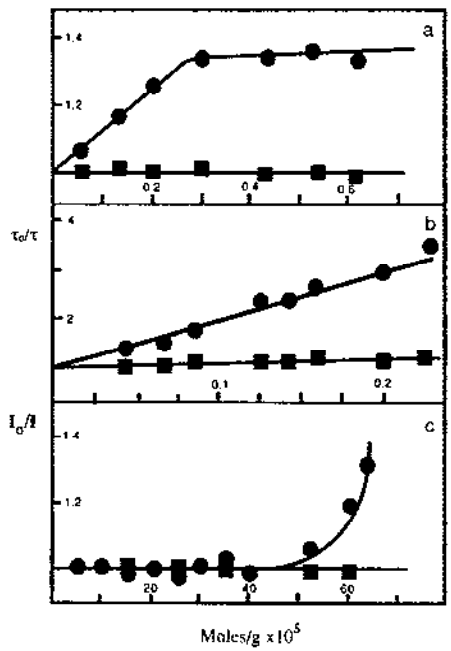

Fig. 5. Relative emission intensities (●) and lifetimes (■) as functions of the moles per gram of (a) Cr^{3+}(ads), (b) Fe^{3+}(ads), and (c) Cu^{2+}(ads).

With ions of low ionic potential and high kinetic lability, the preferred distribution of coadsorbed reagents is one of uniform surface coverage [37]. Cu^{2+} impregnates the interior unoccupied volumes of the glass until the surface coverage in that volume is equivalent to that of $Ru(bpy)_3^{2+}$(ads) in the outermost volumes. The number of Cu^{2+} ions adsorbed into the volumes of glass impregnated with $Ru(bpy)_3^{2+}$(ads) is described in terms of the number of Cu^{2+} ions per $Ru(bpy)_3^{2+}$(ads), n_{Cu}/Ru, by

$$n_{Cu}/Ru=[V_{Ru}/V_T][N_{Cu}/N_{Ru}-(V_{Cu}/V_{Ru})(A_{Ru}/A_{Cu})] \quad (12)$$

where N_{Cu} and N_{Ru} represent the total amounts of Cu^{2+}(ads) and $Ru(bpy)_3^{2+}$(ads) respectively; V_T, V_{Cu} and V_{Ru} denote the total volume of the glass sample, 2500 cm^3, and the volumes of glass occupied by Cu^{2+}(ads) and $Ru(bpy)_3^{2+}$(ads) respectively; A_{Cu} and A_{Ru} are the planar areas of the two adsorbates, which are calculated to be 20 $Å^2$ and 170 $Å^2$ respectively, assuming that the radius of $Ru(bpy)_3^{2+}$(ads) is 7.4 Å and that of Cu^{2+}(ads) is equivalent to that of the hydrated ion, 2.5 Å. Substituting the appropriate values reduces eqn. (12) to

$$n_{Cu}/Ru=0.18[N_{Cu}/N_{Ru}-39] \quad (13)$$

Equation (13) predicts that 2.4×10^{-5} mol Cu^{2+}(ads) per gram must be adsorbed before the onset of $Ru(bpy)_3^{2+}$(ads) quenching. Considering the approximations, particularly the assumption that the size of Cu^{2+}(ads) is equivalent to that of the hydrated ion and the uncertainty in the measured volumes, the predicted value agrees reasonably well with the experiment, which indicates that 5×10^{-5} mol Cu^{2+} per gram must be adsorbed before impregnation of the volumes containing $Ru(bpy)_3^{2+}$(ads) [37].

F. PHOTOREDOX CHEMISTRY

While quenching experiments focus on the formation of the donor–quencher pair, photochemical experiments focus on charge separation. In fact, the first indication that photochemistry on this glass differed from that in fluid solution was a remarkable improvement in charge separation. A 457.9 nm photolysis of $Ru(bpy)_3^{2+}$(ads) in vacuo led to disproportionation

$$2Ru(bpy)_3^{2+}(ads)\rightarrow[Ru(bpy)_2(bpy^-)]^+(ads)+Ru(bpy)_3^{3+}(ads) \quad (14)$$

and optical and ESR experiments showed that the photoredox products persisted for hours after photolysis [46,68]. At the time these experiments were performed, the result was both startling and disconcerting since the driving force for the thermal back reaction, 2.5 eV, is the largest that will be encountered in an $Ru(bpy)_3^{2+}$-photoinduced electron-transfer reaction.

(i) Disproportionation

The absence of either emission or lifetime quenching when $Ru(bpy)_3^{2+}$(ads) cation exchanges onto the glass [41], as well as estimates of the conduction band energy and potential of the glass, based on SiO_2 [69], preclude adsorbate–adsorbent energy transfer or electron transfer to a PVG conduction band [46]. Emission polarization and macroscopic mobility measurements [37,41] indicate that photolysis converts a fixed array of immobilized reactants into a fixed array of immobilized products. The rate of product formation exhibits a second-order dependence on the excitation intensity, and flash photolysis experiments reveal a non-exponential emission decay which, at high excitation intensities, exhibits a distinct minimum. The minimum is due to the absorption of the emission by a transient intermediate. The absorption spectrum of the latter corresponds to that of the hydrated electron, and scavenging experiments confirm its presence [46].

The data suggest the following reaction sequence:

$$Ru(bpy)_3^{2+}(ads) + h\nu \rightarrow {}^*Ru(bpy)_3^{2+}(ads) \quad (15)$$

$${}^*Ru(bpy)_3^{2+}(ads) + h\nu \rightarrow {}^*Ru(bpy)_3^{3+}(ads) + e^- \quad (16)$$

$${}^*Ru(bpy)_3^{2+}(ads) \rightarrow Ru(bpy)_3^{2+}(ads) + h\nu \quad (17)$$

$${}^*Ru(bpy)_3^{2+}(ads) \rightarrow Ru(bpy)_3^{2+}(ads) + \text{heat} \quad (18)$$

$$e^- + Ru(bpy)_3^{2+}(ads) \rightarrow [Ru(bpy)_2(bpy^-)]^+(ads) \quad (19)$$

$$e^- + Ru(bpy)_3^{3+}(ads) \rightarrow {}^*Ru(bpy)_3^{2+}(ads) \quad (20)$$

Reactions (15) and (16) represent sequential excitation through the MLCT state and ionization. Reaction (20) represents the chemiluminescent reduction of the oxidized complex which, in aqueous solution, is diffusion controlled and populates the MLCT state with unit efficiency [47].

Fitting the algorithm derived from the reaction sequence to the time-dependent emission intensity $I(t)$ yields $(1.9 \pm 0.1) \times 10^6\ s^{-1}$ for $k_{17} + k_{18}$. The latter is larger than that obtained from conventional emission decay measurements, $(1.35 \pm 0.04) \times 10^6\ s^{-1}$, but reflects the sensitivity of the algorithm to preceding rapid events which are not at present understood. In contrast with aqueous solution, where reduction of $Ru(bpy)_3^{2+}$ and $Ru(bpy)_3^{3+}$ by the hydrated electron occurs with essentially identical diffusion-controlled rate constants, $(7 \pm 1) \times 10^{10}\ M^{-1}\ s^{-1}$ [47,70–72], the calculated values of k_{19} and k_{20}, $(2.2 \pm 0.1) \times 10^{12}$ and $(2.2 \pm 0.1) \times 10^{13}\ cm^2\ mol^{-1}\ s^{-1}$ respectively suggest that electron transfer on the glass surface responds to the difference in driving force and differentiates the reaction pathways. The differentiation may arise from the fact that the photodetached electron on the glass surface is not actually free, but as described below, appears to reside in surface acceptor sites. If so, reduction of an adsorbate occurs with a concurrent oxidation of the surface acceptor site,

and the driving force for the reaction, and perhaps its rate, reflects the reduction potential of the adsorbate.

The reaction sequence is equivalent to the mechanism of photoinduced disproportionation in aqueous solution except that the reactants and products, which remain cationic throughout the entire sequence, are fixed and the electron is the mobile intermediate. Conduction of the photodetached electron on the glass surface is interpreted within a surface conduction model. We will return to this point in a moment, but within the above model, the quantum yield of $[Ru(bpy)_2(bpy^-)]^+$(ads) formation, Φ_{Rul}, is

$$\Phi_{Rul}=\Phi_p f_{ej} k_{19}/(k_{19}+k_{20}) \tag{21}$$

where Φ_p and f_{ej} represent the quantum yield of photoionization and the fraction of e^- ejected from the surface storage sites respectively. The value of f_{ej} is taken to be unity since the electron is transient. Substitution of the maximum value of Φ_{Rul}, 1.1×10^{-4}, and the calculated values of the rate constants yields 1.2×10^{-3} for Φ_p. Since photoionization of $Ru(bpy)_3^{2+}$(ads) is a sequential biphotonic process, the calculated value of Φ_p is a lower limit. Nevertheless, the value is quite close to the photoionization efficiency in aqueous solution, $(1.5\pm0.2)\times10^{-3}$ [73]. The overall efficiency of disproportionation on this glass is limited principally by the photoionization efficiency and secondarily by the competition between product formation and recombination.

Since the appearance of $Ru(bpy)_2(bpy^-)]^+$(ads) occurs 3 to 4 μs after excitation, and the photodetached electron is detected as an intermediate [46], a significant number of electrons must reside on the glass surface for a finite period of time. Consequently, surface conduction of the photodetached electron is thought to involve the population of intermediate surface acceptor sites. These are thought to be shallow energy wells from which the electron can be thermally activated but, nevertheless, present an energy barrier, albeit slight, that prevents immediate recombination. The nature of the acceptor site is not known, although attractive candidates are the prevalent B_2O_3 Lewis acid sites on the glass surface [46]. These sites could readily accept additional electron density, but in forming a radical-like species, would remain sufficiently reactive to release the electron on thermal activation.

Surface conduction implies that the quantum yield of electron transfer on the glass surface will exhibit an activation barrier that reflects the average depth of the surface acceptor sites. Indeed, Φ_{Rul} increases with increasing temperature in the range 5–65°C, and when corrected for the temperature dependence of the lifetime of $^*Ru(bpy)_3^{2+}$(ads), it yields an activation energy of 6.87 ± 0.11 kcal mol^{-1} [51]. At present, however, the value must be considered tentative. The problem is that photoionization is thought to

occur by a sequential two-photon process; the first photon generates the MLCT state which then absorbs the second photon. Therefore a critical parameter is η_{isc}, and in calculating the activation energy, it was assumed to be independent of temperature [51]. However, subsequent measurements, described in the section on excited state dynamics, reveal that the product $\eta_{isc}k_r$ for $Ru(bpy)_3^{2+}$(ads) declines with increasing temperature. It is important to realize that $\eta_{isc}k_r$ declines with increasing temperature, whereas Φ_{RuI} increases with temperature. If the entire temperature dependence of $\eta_{isc}k_r$ is attributed solely to η_{isc}, however, the activation energy increases only slightly. Consequently the above value, if not exact, is a reasonable estimate of the actual activation energy.

The value of Φ_{RuI} depends on the photoionization efficiency and the rates of reduction of $Ru(bpy)_3^{2+}$(ads) and $Ru(bpy)_3^{3+}$(ads) by the photodetached electron. Since kT at 90°C, 0.16 eV, is considerably smaller than the excitation energy required for ionization, $2.2 \leqslant E \leqslant 5.0$ eV [46,51], the ionization efficiency is taken to be independent of temperature. Since the driving forces for reactions (19) and (20) are 1.5 eV and 4.0 eV respectively, their rate constants are also assumed to be independent of temperature. Consequently the measured activation energy principally reflects energy barriers encountered during electron transport on the glass surface. Within the proposed surface conduction model, this suggests that the average depth of the surface acceptor site(s) is equal to or less than 6.87 ± 0.11 kcal mol^{-1} [51].

Photoinduced disproportionation on this glass occurs within a fixed array of immobilized reactants by means of mobile photodetached electrons. Thus the dependence of quantum efficiency, Φ_{RuI} on the moles adsorbed per gram (Fig. 6) is interpreted in terms of the mean separation between reactants and products. As the moles adsorbed per gram increases, the mean separation between the adsorbed ions decreases and approaches a separation distance within the electron migration distance. Consequently the probability of reaction (19) increases. The maximum yield corresponds to a mean electron migration distance of 50 ± 10 Å. The value is in excellent agreement with a reported value of 49 Å and an estimate of 30 Å for the mean electron migration distance in PVG [74,75]. Furthermore, although electrical conductivity of amorphous solids depends on the method of preparation, surface structure and surface impurities, the value is similar to the 34 Å electron migration distance in SiO_2 [76]. The separation between the disproportionation products, however, exceeds that for the thermally activated reverse reaction. The latter is either restricted or curtailed, and the quantum efficiency of disproportionation initially increases. Further increases in the moles adsorbed per gram decrease the mean separation between the disproportionation products and increase the probability of the reverse reaction. Consequently the net efficiency declines. The reverse re-

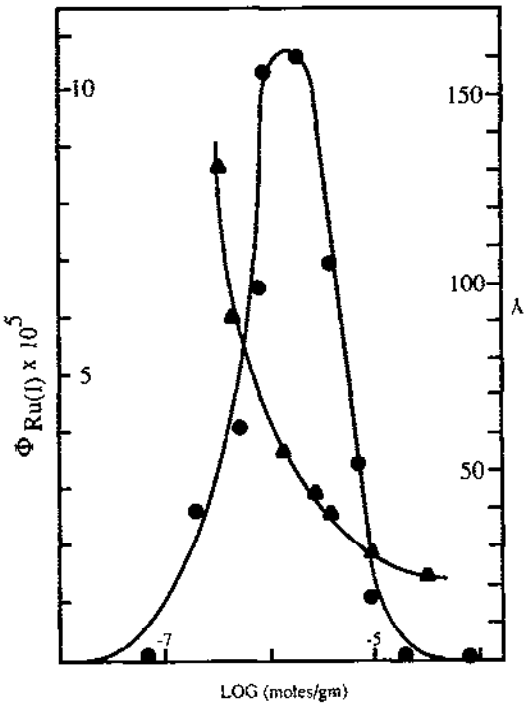

Fig. 6. Dependence of Φ_{RuI} (●) on the moles of $Ru(bpy)_3^{2+}$(ads) per gram, and the calculated mean separation between the adsorbed ions (▲).

action dominates, i.e. Φ_{RuI} approaches zero, when the loading exceeds 2×10^{-5} mol g^{-1}. This corresponds to a mean Ru–Ru separation of 20 ± 10 Å which indicates that the distance between the coordination shells must be 13 Å or less for the thermal back reaction to occur. This result is in reasonable agreement with the distance dependence found in the thermal reactions between $Ru(bpy)_3^{3+}$ and methylviologen homologues. In glycerol at 0°C, the latter reactions require a mean separation ranging from a contact interaction to 10 Å [77].

(ii) Photoreduction of methylviologen

A 450 nm photolysis of glasses containing coadsorbed $Ru(bpy)_3^{2+}$(ads) and methylviologen, MV^{2+}(ads), yields the radical cation MV^{+}(ads), which is also stable for at least 30 min after photolysis [78]. The electronic spectrum of MV^{+}(ads) agrees with the spectrum of MV^{+}(ads) generated chemically, and disappears immediately on exposure to air. As in the disproportionation reaction, product stability is a consequence of the glass surface. Both reagents undergo cation exchange onto the glass surface and the surface

defines an array of immobilized reactants, which photolysis converts to immobilized products [78]. However, the spatial array of adsorbates, and therefore the dependence on moles adsorbed, is defined by a partitioning of $Ru(bpy)_3^{2+}$(ads) and MV^{2+}(ads) within the glass matrix.

Although markedly different in molecular structure, the distribution of coadsorbed MV^{2+} closely resembles that of coadsorbed Cu^{2+}(ads) (see above) [37]. $Ru(bpy)_3^{2+}$ impregnates the outermost volumes of the glass, whereas MV^{2+} diffuses into the interior and impregnates the unoccupied volumes [78]. Consequently, quenching does not occur and photolysis does not lead to net reaction. As the moles adsorbed increase, MV^{2+} begins to impregnate the outermost volumes containing $Ru(bpy)_3^{2+}$(ads). Within a narrow range of moles adsorbed per gram, where MV^{2+}(ads) begins to impregnate the volumes of glass containing the complex, 450 nm photolysis leads to MV^{+}(ads) formation. MV^{+}(ads) formation does not occur throughout the entire volume impregnated with $Ru(bpy)_3^{2+}$, but only in the boundary regions containing both reagents [78].

Photoexcitation of $Ru(bpy)_3^{2+}$(ads) initiates the reaction, but the absence of MV^{2+} quenching under the conditions that lead to MV^{+}(ads) formation precludes direct oxidative quenching. Rather, MV^{+}(ads) formation is thought to occur by photoionization of $Ru(bpy)_3^{2+}$(ads). The mobile photodetached electron then reduces MV^{2+}(ads) within the electron migration distance of 50 ± 10 Å [46]. Since this distance exceeds the distance for the thermal back reaction, 10 Å or less, the redox products are stable. The spectral data also indicate the formation of $[Ru(bpy)_2(bpy^{\cdot-})]^{+}$(ads). Since the oxidation potential of the latter, 1.3 V, exceeds the reduction potential of MV^{2+}, -0.44 V, MV^{+}(ads) formation may also arise from the secondary thermal reaction

$$[Ru(bpy)_2(bpy^{-})]^{+} + MV^{2+} \rightarrow Ru(bpy)_3^{2+} + MV^{+} \tag{22}$$

We suspect that the secondary reaction requires essentially a contact interaction. However, it is not burdened by an exergonic back reaction, and its occurrence promotes product stability by reducing the driving force for the back reaction from 2.5 eV for the disproportionation products to 1.6 eV for the $Ru(bpy)_3^{3+}$–MV^{+} reaction.

G. SUMMARY

The differences between behavior in fluid solution and behavior that occurs on this glass are not a consequence of a molecular change. With few exceptions [40] the spectroscopic properties of molecules, whether cation exchanged or physisorbed [33,34,38] onto this glass, are equivalent to those

found in fluid solution. In essence, the differences from fluid solution behavior arise either from the rigidity of the support or from a severe curtailment of molecular mobility. Particularly with ruthenium(II) diimmines, where the excited state chemistry is dominated by bimolecular events, the elimination of diffusion randomization changes both the formation of the donor–quencher pair and the subsequent thermal chemistry from that dependent simply on amount to that dependent on the spatial array of adsorbates either within the glass matrix or amongst the phases in contact with the glass matrix.

The net photoredox chemistry observed on this glass initiates with a two-photon ionization of $Ru(bpy)_3^{2+}$(ads). The photodetached electron is a mobile intermediate within a fixed array of immobilized reactants. Electron conduction is thought to occur by a surface conduction mechanism in which the photodetached electron populates surface acceptor sites. These are shallow energy wells, equal to or less than 6.87 ± 0.11 kcal mol^{-1}, from which the electron can be thermally released, but they present a barrier to immediate recombination. A net redox chemistry occurs when the distance between the adsorbates is less than the electron migration distance of 50 ± 10 Å but greater than that required for the thermal back reaction.

Obviously the initiating and conduction steps depend on the nature of the support. On a semiconductive metal oxide, for example, one-photon excitation of $Ru(bpy)_3^{2+}$(ads) results in population of the conduction band, via oxidative quenching of the adsorbate, and the conduction band allows electron migration. Nevertheless, there are a number of similarities. Band bending in a semiconductor curtails immediate charge recombination [69] in much the same manner that the depth of the surface acceptor site presents a barrier to recombination on the glass surface. Furthermore, since the surfaces of many metal oxides are anionic, most probably the adsorbates, particularly cationic adsorbates, are immobilized on the surface, and the electron is the mobile intermediate. In the absence of an applied potential, the probability of a net chemistry, as on the glass surface, depends on the probability of the electron encountering a secondary reaction site relative to the probability of the back reaction. In this sense, both depend on the spatial array of the adsorbates, i.e. the mean spacing between the adsorbates must be within the electron migration distance, but the latter must exceed that required for the thermal back reaction.

ACKNOWLEDGMENT

Support of this research by the Research Foundation of the City University of New York, the New York State Science and Technology Foundation

and the National Science Foundation (CHE-8511727) is gratefully acknowledged. We also thank Dr. David L. Morse of the Corning Glass Works for many valuable discussions and the samples of porous Vycor glass.

REFERENCES

1 H.D. Gafney and A.W. Adamson, J. Am. Chem. Soc., 94 (1972) 8238.
2 (a) K. Kalyanasundram, Chem. Soc. Rev., 7 (1978) 453; Coord. Chem. Rev., 46 (1982) 159. (b) A. Juris, V. Balzani, F. Barigelletti, S. Campagna, P. Belser and A. von Zelewsky, Coord. Chem. Rev., 84 (1988) 85.
3 G.A. Somorjai, Chemistry in Two Dimensions: Surfaces, Cornell University Press, Ithaca, NY, 1981, Chapter 1.
4 I. Willner and Y. Degani, J. Am. Chem. Soc., 105 (1983) 6228.
5 J. Wheeler and J.K. Thomas, J. Phys. Chem., 86 (1982) 4540.
6 I. Willner, J.W. Otvos and M.J. Calvin, J. Am. Chem. Soc., 103 (1981) 3203.
7 J.K. Thomas, Chem. Rev., 80 (1980) 283; J. Phys. Chem., 91 (1987) 267.
8 T. Matsuo, K. Takuma, T. Nishizima and Y. Tsutsui, J. Coord. Chem., 10 (1980) 195.
9 B.H. Milosavijevic and J.K. Thomas, J. Phys. Chem., 87 (1983) 616.
10 M. Gratzel, Acc. Chem. Res., 14 (1981) 376.
11 N. Vlachopoulos, P. Liska, J. Augustynski and M. Gratzel, J. Am. Chem. Soc., 110 (1988) 1216.
12 J.M. Lehn, J.P. Sauvage and R. Ziessel, Nouv. J. Chim., 4 (1980) 623.
13 W.D. Clark and N. Sutin, J. Am. Chem. Soc., 99 (1977) 4676.
14 A.J. Novak, in J.S. Connolly (Ed.), Photochemical Conversion and Storage of Solar Energy, Academic Press, New York, 1981, p. 271; Appl. Phys. Lett., 30 (1977) 567.
15 J.S. Krueger, J.E. Mayer and T.E. Mallouk, J. Am. Chem. Soc., 110 (1988) 8232.
16 Z. Li, C. Lai and T.E. Mallouk, Inorg. Chem., 28 (1989) 178.
17 N.B. Hannay, Solid State Chemistry, Prentice-Hall, Englewood Cliffs, NJ, 1967, Chapters 1 and 2.
18 T.H. Elmer, J. Am. Ceram. Soc., 53 (1970) 171.
19 E.A. Mendoza, E. Wolkow, H.D. Gafney, D. Sunil, M. Rafailovich, J. Sokolov, G.C. Long and P.R. Jemian, Appl. Phys. Lett., submitted.
20 A.L. Spatorico, J. Appl. Polym. Sci., 12 (1975) 1601.
21 R.K. Iler, The Chemistry of Silica, Wiley-Interscience, New York, 1979, pp. 551, 622.
22 J.A. Hockey, Chem. Ind. (London), (1965) 57.
23 Y. Davydov, Trans. Faraday Soc., 60 (1964) 2254; Russ. J. Phys. Chem., 38 (1964) 1108.
24 V.F. Janowski and E. Heyer, Z. Chem., 19 (1979) 1.
25 K.G. All, J. Organomet. Chem., 87 (1975) 203.
26 D.N. Strazhesko, J. Chromatogr., 102 (1974) 191.
27 F. Vydra and M. Markova, J. Inorg. Nucl. Chem., 26 (1964) 1319.
28 S. Arhland, I. Grenthe and B. Noren, Acta Chem. Scand., 14 (1960) 1059.
29 L.R. Snyder and J.W. Ward, J. Phys. Chem., 70 (1966) 3941.
30 A.N. Sidorov, Opt. Spektrosk. (Akad. Nauk SSSR, Otd. Fiz.-Mat. Nauk), 8 (1960) 424 (English translation).
31 N.W. Cant and L.H. Little, Can. J. Chem., 42 (1964) 802; 43 (1965) 1252.
32 T.H. Elmer, I.D. Chapman and M.E. Nordberg, J. Phys. Chem., 66 (1962) 1517.
33 T. Dieter and H.D. Gafney, Inorg. Chem., 27 (1988) 1730.
34 M.S. Darsillo, M.S. Paquette and H.D. Gafney, J. Am. Chem. Soc., 109 (1987) 3275.
35 A. Basu, D.J. Perettie, J.B. Clark and H.D. Gafney, J. Phys. Chem., 87 (1983) 4532.
36 H.W. Goonatilakie, Ph.D. Thesis, City University of New York, 1986.

37 W. Shi and H.D. Gafney, J. Phys. Chem., 92 (1988) 2329.
38 R.C. Simon, E.A. Mendoza and H.D. Gafney, Inorg. Chem., 27 (1988) 2733.
39 T. Kennelly, Ph.D. Thesis, City University of New York, 1980.
40 T.C. Strekas, H.W. Goomatilake and H.D.Gafney, Inorg. Chem., 24 (1985) 4439.
41 W. Shi, S. Wolfgang, T.C. Strekas and H.D. Gafney, J. Phys. Chem., 89 (1985) 974.
42 A. Washel, Annu. Rev. Biophys. Bioeng., 6 (1977) 273.
43 S. Tysoe, J. Fan and H.D. Gafney, unpublished observation, 1988.
44 S. Wei, J.B. Clark, D.J. Perettie and H.D. Gafney, Chem. Phys. Lett., 99 (1983) 253.
45 J. Wheeler and J.K. Thomas, J. Phys. Chem., 86 (1982) 4540.
46 T. Kennelly, M. Braun and H.D. Gafney, J. Am. Chem. Soc., 107 (1985) 4431.
47 J.E. Martin, E.J. Hart, A.W. Adamson, H.D. Gafney and J. Halpern, J. Am. Chem. Soc., 94 (1972) 9238.
48 J. Van Houten and R.J. Watts, J. Am. Chem. Soc., 98 (1976) 4853.
49 S.R. Allsopp, A. Cox, T.J. Kemp and W.J. Reed, J. Chem. Soc., Faraday Trans. 1, 74 (1978) 1275; Chem. Phys. Lett., 43 (1976) 135.
50 W.M. Wacholtz, R.C. Auerbach, R.H. Schemehl, M. Ollino and W.R. Cherry, Inorg. Chem., 23 (1984) 938; 24 (1985) 1758.
51 J. Fan, W. Shi, S. Tysoe, T.C. Strekas and H.D. Gafney, J. Phys. Chem., 93 (1989) 373.
52 J.N. Demas and G.A. Crosby, J. Am. Chem. Soc., 93 (1971) 2841.
53 D. Ege, P.K. Ghosh, J.R. White, J.F. Eqney and A.J. Bard, J. Am. Chem. Soc., 107 (1985) 5644.
54 R.A. DellaGuardia and J.K. Thomas, J. Phys. Chem., 87 (1983) 990, 3550.
55 S. Wolfgang and H.D. Gafney, J. Phys. Chem., 87 (1983) 5395.
56 J.N. Demas, D. Diemente and E.W. Harris, J. Am. Chem. Soc., 95 (1973) 6864.
57 V.S. Srinivasan, D. Podolski, N.J. Westrick and D.C. Neckers, J. Am. Chem. Soc., 100 (1978) 6513.
58 H. Sponer and L.G. Bonner, J. Chem. Phys., 8 (1940) 33.
59 J.C.D. Brand, V.T. Jones and C. DiLauro, J. Mol. Spectrosc., 45 (1973) 404.
60 P.W. Atkins, Physical Chemistry, W.H. Freeman, San Francisco, CA, 1978, p. 804.
61 J.M. Frank and S.I. Vavilov, Z. Phys., 69 (1931) 100.
62 S. Siegel and H.S. Judeikis, J. Chem. Phys., 48 (1968) 1613.
63 E.J. Bowen and W.S. Metcalf, Proc. R. Soc. London, Ser. A, 206 (1951) 937.
64 J.R. Miller, K.W. Hartman and S. Abrash, J. Am. Chem. Soc., 104 (1982) 4286.
65 L. Sacconi, Discuss. Faraday Soc., 7 (1949) 173.
66 F.H. Burstall, G.R. Davies and R.A. Wells, Discuss. Faraday Soc., 7 (1949) 179.
67 B. Douglas, D. McDaniel and J.J. Alexander, Inorganic Chemistry, 2nd edn., Wiley, New York, 1983, Chapter 9.
68 T. Kennelly and H.D. Gafney, J. Inorg. Nucl. Chem., 43 (1980) 2988.
69 T. Kajiwara, K. Hasimoto, T. Kawai and T. Sakata, J. Phys. Chem., 86 (1982) 4516.
70 J.H. Baxendale and M. Fiti, J. Chem. Soc., Dalton Trans., (1972) 1995.
71 Q.G. Mulazzani, S. Emmi, P.G. Fouchi, M. Ventur and M.Z. Hoffman, J. Am. Chem. Soc., 100 (1978) 1978.
72 D. Meisel, M.S. Matheson and J. Rabini, J. Am. Chem. Soc., 100 (1978) 117.
73 D. Meisel, M.S. Matheson, W.A. Mulac and J. Rabini, J. Phys. Chem., 81 (1977) 1449.
74 P.K. Wong, Photochem. Photobiol., 19 (1974) 391.
75 P.K. Wong and A.O. Allen, J. Phys. Chem., 74 (1970) 774.
76 C.N. Burgland and R.J. Powell, J. Appl. Phys., 42 (1971) 573.
77 T. Guarr and C. McLendon, Abstr., 182nd Nat. Meet. Am. Chem. Soc., New York, 1981, INORG 20.
78 W. Shi and H.D. Gafney, J. Am. Chem. Soc., 109 (1987) 1582.
79 F. Felix, J. Ferguson, H.U. Gudel and A. Ludi, J. Am. Chem. Soc., 102 (1980) 4096.
80 L.F. Fieser and M. Fieser, Advanced Organic Chemistry, Reinhold, New York, 1961, p. 847.